

Estimator Based Multi-Eigenmode Control of Cantilevers in Multifrequency Atomic Force Microscopy

Andreas Schuh^{1,2}, Iman Soltani Bozchalooi¹, Ivo W. Rangelow² and Kamal Youcef-Toumi¹

Abstract—Today, multifrequency Atomic Force Microscopy is a popular technique to extract properties of a sample surface other than the topography through different channels. Such channels are represented by the higher eigenmodes and harmonics of the flexural vibrations of the cantilever. In one method two or more eigenmodes are actuated simultaneously, whereas another method captures the harmonics excited from the first eigenmode tapping the surface. In this paper, we present a compensation strategy to modify the dynamics of two transverse eigenmodes independently. The modeling, compensator design, implementation and imaging performance on a polymer sample is outlined. In particular low Q factors in the first and high Q factors in the second eigenmode indicate a strong improvement in material contrast mapping. As the imaging bandwidth depends on the Q factor of the first eigenmode, the imaging rate is increased simultaneously.

I. INTRODUCTION

The Atomic Force Microscope (AFM) has become a versatile and powerful tool to investigate nanoscale processes. Technical advances and new methods allow imaging the topography and other surface characteristics in real-time. For example, observation of fast dynamics of biological processes or covering large areas on wafers require a high speed operation. The advancements have also made AFMs more affordable than ever.

Both imaging rate and force sensitivity are important factors in the AFM. The imaging rate is limited by scanner resonances, electronics, amplifiers, control feedback loop and the cantilever probe [1, 2]. The imaging bandwidth of the cantilever itself can be expressed in terms of an effective Q factor and resonance frequency. Variations in the sample structure are slowly picked up by high Q factored cantilevers [3]. Cantilevers are often manufactured from materials with very low internal damping. Even in ambient pressure the Q factors are

typically up to 500 with time constants of several milliseconds, forming a bottleneck in the system. In contrast, high Q factors are often required for gentle imaging.

Faster cantilevers can be achieved through control means [3] or by appropriate structural design. The structural modifications can include an increased thickness, decreased length or different materials. These measures can increase the resonance frequency or intrinsic damping [4, 5]. Dimensional adjustments are bound to a modification of the fabrication process, which is expensive and time consuming. In contrast, active control is an alternative approach, where e.g. the damping of the cantilever is varied by feedback control [6, 7]. Q control can be easily incorporated into existing systems. In the past, Q control has been applied in various applications for cantilevers in the first eigenmode, mainly for increased imaging sensitivity. In contrast, the increased damping allows lower Q factors for high speed imaging [3].

At the same time, mapping material properties is of high interest. Traditional methods involve mapping the phase signal of the fundamental resonance. The phase is sensitive to compositional variations of the sample and is usually accounted to the dissipative tip-sample interaction [8, 9]. Here, the Q factor influences the sensitivity towards material properties. Using higher cantilever eigenmodes has further improved the sensitivity to compositional variations [10, 11].

Modern methods of material sensitive imaging involve two or more cantilever eigenmodes at a time in a multi-frequency approach [12]. Two major methods exist, where in both cases the first eigenmode is used for topography feedback mapping of the sample. In one method one (bimodal) or several higher eigenmodes are actuated simultaneously with the first eigenmode [13, 14]. The higher sensitivity of the higher eigenmodes' amplitudes and phases is then used to locally quantify e.g. the Young's modulus. In the second method, the excited higher harmonics are extracted that appear due the tip periodically and intermittently touching the sample surface [15, 16]. Based on the periodicity of the tip-sample force, it can be expanded into a Fourier series [17, 18]. The magnitudes of each harmonic force depends on the contact time of the tip with the sample surface. Mapped with the cantilever transfer function, the response is more or less attenuated depending on the vicinity of nearby eigenmodes. Usually, a reference material with known properties is also measured and then compared to the sample under investigation.

This work was supported by the Singapore-MIT Alliance, European Union's Seventh Framework Programme FP7/2007-2013 under grant agreement no. 318804 (SNM) and ZIM-Project KF2114205NT2. A. S. thanks the German Academic Exchange Service (DAAD) for fellowship support under contract D/09/45781.

¹Massachusetts Institute of Technology, Department of Mechanical Engineering, 77 Massachusetts Avenue, Cambridge, MA 02139, USA. A.S.: aschuh@mit.edu, I.S.B.: isoltani@mit.edu, K.Y.T.: youcef@mit.edu

²Ilmenau University of Technology, Faculty of Electrical Engineering and Information Technology, Dept. of Microelectronic and Nanoelectronic Systems, Gustav-Kirchhoff-Str. 1, 98684 Ilmenau, Germany I.W.R.: ivo.rangelow@tu-ilmenau.de

A combination of multifrequency AFM techniques and Q control is appealing. Few attempts have been previously reported to involve and control higher AFM cantilever eigenmodes simultaneously. However, these did not address the multi-frequency imaging aspects, in particular towards material contrasts. Such work includes the first two transverse eigenmodes. The topography is imaged with the Q controlled first [19] or second eigenmode [20]. At the same time the other eigenmode is suppressed to prevent its undesired excitation.

In this work, a novel method combining multi-eigenmode control and multifrequency AFM techniques is introduced. An estimator based compensator is connected to the cantilever as a feedback system. The cantilevers' different eigenmodes of vibration can then be modified concurrently and independently. The modified AFM setup shown in Fig. 1 is utilized in this work. It is a standard setup that is extended by new signal paths, the multi-eigenmode compensator and a second Lock-in amplifier, represented by dashed lines and boxes. The signals of the second Lock-in amplifier are plotted alongside with the topography and phase that correspond to the first eigenmode. The cantilevers utilized have integrated thermal expansion based bimorph actuation and displacement proportional piezo-resistive sensors [21, 22].

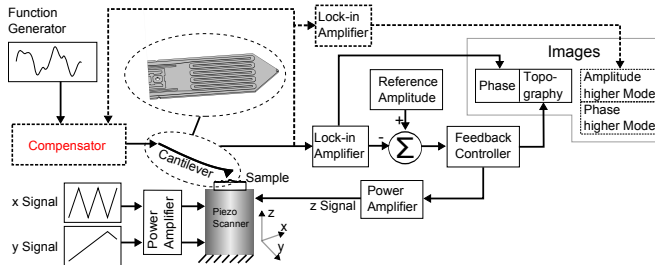


Fig. 1: Modified AFM setup for multi-eigenmode control. Dashed lines and boxes indicate the modification of the standard setup.

The paper is organized as follows. In Section II, a cantilever multi-eigenmode model is derived. The model based compensator design is presented in Section III. In Section IV, the compensator's discrete implementation is outlined, which is then used during imaging in Section V. A conclusion is given in Section IV.

II. CANTILEVER MODELING

In this section, a sufficient model of the cantilever dynamics is obtained based on measurements. It includes the first and higher transverse eigenmodes and supports the compensator design in Section III. The output of the linear model is proportional to the tip displacement upon a harmonic input signal. As modal superposition can be assumed for small amplitudes, the model is a sum of each individual eigenmode. The cantilever to be modeled can

be represented in the form

$$\dot{\mathbf{q}}(t) = \mathbf{A}\mathbf{q}(t) + \mathbf{B}u(t) + w(t), \quad (1)$$

$$y(t) = \mathbf{C}\mathbf{q}(t) + Du(t) + v(t), \quad (2)$$

where \mathbf{A} is the state transition matrix incorporating the cantilever dynamics, \mathbf{B} the state input vector, \mathbf{C} the state measurement vector and D the direct feed-through, where all have constant parameters in the linear model. $w(t)$ and $v(t)$ represent the process and measurement noise, respectively. Equation (2) gives an expression for the measurements $y(t)$ in terms of the variables $\mathbf{q}(t)$, input $u(t)$ and measurement noise $v(t)$.

The model of the cantilever is estimated in the frequency domain through a system identification using the Prediction Error Method (PEM) [23]. The procedure can be carried out automatically, as it is necessary after every change of cantilever or environment. The estimated matrices can be expressed as

$$\bar{\mathbf{A}} = \begin{bmatrix} \bar{\mathbf{A}}_1 & \mathbf{0} & \cdots \\ \mathbf{0} & \bar{\mathbf{A}}_2 & \\ \vdots & & \ddots \end{bmatrix}, \bar{\mathbf{B}} = \begin{bmatrix} \bar{\mathbf{B}}_1 \\ \bar{\mathbf{B}}_2 \\ \vdots \end{bmatrix}, \bar{\mathbf{C}} = \begin{bmatrix} \bar{\mathbf{C}}_1 \\ \bar{\mathbf{C}}_2 \\ \vdots \end{bmatrix}^T, \quad (3)$$

where $\bar{\mathbf{A}}$, $\bar{\mathbf{B}}$ and $\bar{\mathbf{C}}$ are the experimentally determined matrices/vectors of \mathbf{A} , \mathbf{B} and \mathbf{C} , respectively. Each of them contains sub-matrices/vectors representing a modeled eigenmode, indicated by the indexes. The block diagonal modal representation is suitable for the hardware implementation that will be discussed in Section 4. The term $Du(t)$ is objected in Equation (3). However, it could be used to separately model the cantilever's cross-talk of the actuation signal onto the piezo-resistive sensors. The Q factor and natural frequency of each eigenmode can be found through the eigenvalues of the estimated model.

As shown via experimental results in Section V the linear model is robust in imaging the different samples and in presence of the non-linear tip-sample interactions.

III. COMPENSATOR DESIGN

The design based on a full state feedback controller and prediction estimator is introduced in the following. The controller design is presented first, assuming full access to the state variables of the cantilever. The estimator is derived thereafter, giving access to the unmeasured tip velocity. Both controller and estimator are combined to form the overall compensator that is connected to the cantilever as a feedback.

A. Controller

The complex conjugate pole pair of each modeled eigenmode can be arbitrarily and independently moved in the complex plane. Based on the model of Equation (3), it offers the possibility to modify the Q factor Q_i and/or natural frequency $\omega_{n,i}$ of the i^{th} eigenmode. A

controller \mathbf{K} is incorporated with the actuation signal r to form the new cantilever input u_k as

$$u_k = -\mathbf{K}\mathbf{q}_k + Nr_k. \quad (4)$$

N can be used to eliminate the steady state error introduced by the state feedback.

The dynamics of each eigenmode are modified either towards a desired Q factor $Q_{des,i}$, desired natural frequency $\omega_{n_{des,i}}$ or both simultaneously. A desired conjugate complex $p_{i,1,2}$ pole pair can be found by the relationship

$$p_{i,1,2} = \omega_{n_{des,i}} \left(-\frac{1}{2Q_{des,i}} \pm \sqrt{\frac{1}{4Q_{des,i}^2} - 1} \right). \quad (5)$$

The choices of $\omega_{n_{des,i}}$ and $Q_{des,i}$ determine the dynamic modification of each resonance:

- (A) By substitution of $\omega_{n_{des,i}} = \omega_{n,i}$ and choosing $Q_{des,i}$, each eigenmode can be modified in its Q factor only. Here, $\omega_{r,i}$ naturally changes with varying closed loop $Q_{des,i}$ based on $\omega_{r,i} = \omega_{n,i} \sqrt{1 - 1/(2Q_{des,i}^2)}$. A variation of $Q_{des,i}$ in a sweep fashion causes the pole pairs to form a circular movement in the complex plane (Fig. 2(a)). It starts close to the imaginary axis for high $Q_{des,i}$ and meets the negative real axis in the critically damped case of low $Q_{des,i}$. An increase of $Q_{des,i}$ moves the poles closer to the imaginary axis, potentially leading to instabilities,
- (B) By substitution of $Q_{des,i} = Q_i$ and choosing $\omega_{n_{des,i}}$, each eigenmode can be modified in its natural frequency only. Fig. 2(b) indicates the formation of such poles in the complex plane with a sweep of $\omega_{n_{des,i}}$,
- (C) By choosing both $Q_{des,i}$ and $\omega_{n_{des,i}}$ a dynamic behavior can modify the pole locations arbitrarily.

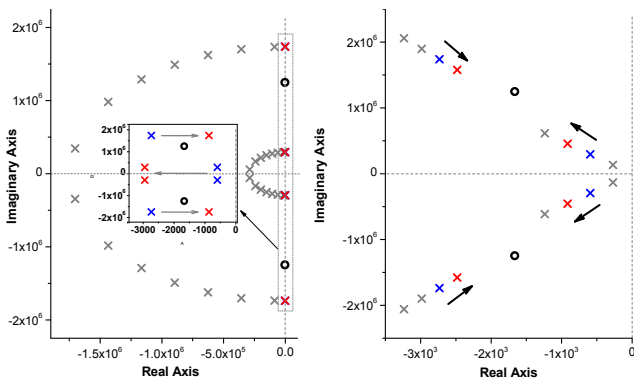


Fig. 2: The modification of (a) Q_i and (b) $\omega_{n,i}$ in a sweep of $Q_{des,i}$ and $\omega_{n_{des,i}}$, respectively. As indicated by arrows in the inset of (a), Q_1 is increased and Q_2 is decreased. The zeros remain unaffected.

Arbitrarily placed pole pairs are often not practicable. Increasing the Q factors towards very high values is prone

to instabilities due to positive feedback of the compensator. In contrast, very low Q factors can be unfeasible as the resonance curves become flat. The maximum control action is mostly limited by the cantilever's actuator.

B. Estimator

A full state estimator is chosen to estimate both the unmeasured velocity and measured displacement of the tip vibrations. Including the latter one improves the noise in the system. The tip velocity is required as it can directly affect the Q_i of the eigenmodes. Specifically, a steady state Kalman filter is used. To maximize sampling rates, the estimator is set up in the predictive form with its discrete time representation

$$\hat{\mathbf{q}}_{k+1} = \bar{\mathbf{A}}\hat{\mathbf{q}}_k + \bar{\mathbf{B}}u_k + \mathbf{L}(y_k - \hat{y}_k). \quad (6)$$

The states $\hat{\mathbf{q}}_k$ are estimates of the states \mathbf{q}_k . $\hat{y}_k = \bar{\mathbf{C}}\hat{\mathbf{q}}_k$ and $y_k = \mathbf{C}\mathbf{q}_k + v_k$ are the estimated and measured cantilever displacement signal, respectively. y_k with its noise v_k forms one of the two inputs to the estimator and is multiplied by the estimator gain \mathbf{L} . Thus, higher gains result in faster poles that improve convergence, but also amplify the noise effects.

C. Combined Controller, Estimator and Cantilever

The controller of Section A is combined with the estimator of Section B and the resulting compensator connected to the cantilever. Hence, \mathbf{q}_k of Equation (4) is replaced by the state estimates $\hat{\mathbf{q}}_k$ of Equation (6):

$$u_k = -\mathbf{K}\hat{\mathbf{q}}_k + Nr_k. \quad (7)$$

Combination of controller and estimator results in

$$\hat{\mathbf{q}}_{k+1} = (\bar{\mathbf{A}} - \bar{\mathbf{B}}\mathbf{K} - \mathbf{L}\bar{\mathbf{C}})\hat{\mathbf{q}}_k + \mathbf{B}Nr_k + \mathbf{L}y_k, \quad (8)$$

which is combined with the cantilever's dynamics to form

$$\begin{bmatrix} \mathbf{q}_{k+1} \\ \hat{\mathbf{q}}_{k+1} \end{bmatrix} = \begin{bmatrix} \mathbf{A} & -\mathbf{B}\mathbf{K} \\ \mathbf{L}\mathbf{C} & \bar{\mathbf{A}} - \bar{\mathbf{B}}\mathbf{K} - \mathbf{L}\bar{\mathbf{C}} \end{bmatrix} \begin{bmatrix} \mathbf{q}_k \\ \hat{\mathbf{q}}_k \end{bmatrix} + \begin{bmatrix} \mathbf{B}N \\ \bar{\mathbf{B}}N \end{bmatrix} r_k + \begin{bmatrix} \mathbf{B} \\ 0 \end{bmatrix} w_k + \begin{bmatrix} 0 \\ \mathbf{L} \end{bmatrix} v_k, \quad (9)$$

$$\begin{bmatrix} y_k \\ \hat{y}_k \end{bmatrix} = \begin{bmatrix} \mathbf{C} & 0 \\ 0 & \bar{\mathbf{C}} \end{bmatrix} \begin{bmatrix} \mathbf{q}_k \\ \hat{\mathbf{q}}_k \end{bmatrix} + \begin{bmatrix} 1 \\ 0 \end{bmatrix} v_k. \quad (10)$$

The output equation $[y_k \hat{y}_k]^T$ holds the cantilever sensor and estimated measurement. Fig. 3 is a block diagram presenting the combined compensator and cantilever setup according to Equations (9) and (10).

IV. IMPLEMENTATION

The compensator is implemented digitally into two different Field Programmable Gate Array (FPGA) platforms with fast Analog-to-Digital (ADC) and Digital-to-Analog Converters (DAC), using a state machine structure and floating point representation. The first platform is a National Instruments (NI) FlexRIO PXI-7954R board equipped with a Virtex 5 LX-110 FPGA

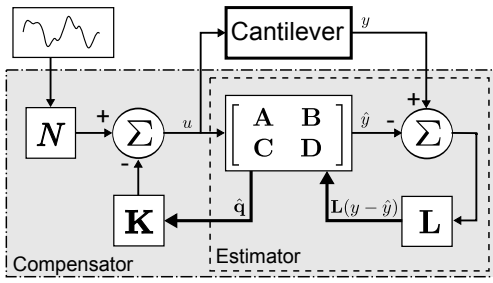


Fig. 3: The compensator connected to the active cantilever and external actuation.

and programmed with NI LabVIEW FPGA. A Baseband Transceiver 5781 with 100 MHz ADCs/DACs is connected for fast sampling. The second platform is a Trenz Electronic board with a Spartan-3A DSP, placed on a custom Hardware board equipped with 100 MHz converters and configured with VHDL. The preceding PEM system identification is performed off-line by first recording the output based on a known input signal. Both are then processed in MATLAB.

The compensator loop rate (Fig. 4) determines the overall feedback bandwidth. It is executed and computed by different, faster loops that are capturing new samples, computing the consecutive control action and form the new actuation signal. The path with the highest delay in the design determines the maximum possible clock and hence compensator loop rate. The implementation is using floating point arithmetic that greatly increase the dynamic range.

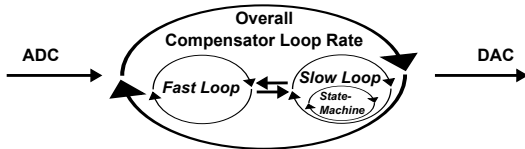


Fig. 4: Brief overview of the implementation.

The *Fast Loop* in Fig. 4 performs tasks such as AD and DA conversion, decimation/interpolation, fixed-point/floating-point conversion and buffering samples in a FIFO for clock domain crossings. The *Slow Loop* performs the compensator calculation with a state machine.

A state machine is chosen for two reasons. First, hardware components can be reused and assigned with different tasks each state iteration. This saves potentially valuable space and components inside the FPGA, such as the XtremeDSP DSP48 Slices. Second, splitting the computation into many steps allows higher clock rates that otherwise introduces long signal paths. Our experience has shown that the depth of pipelining and achieved clock rate has a point of optimum trade-off, where the resulting compensator loop rate is maximized. The state machine is organized such that new incoming samples can be processed as quickly as possible to reduce the compensator time delay. The calculation of the updated

cantilever actuation signal u in time step k is the first computation performed after a new incoming sample. All remaining compensator computations that are needed for time step $k + 1$ are not dependent on a consecutive incoming sample. Hence, the computations influencing time step $k + 1$ can be carried out during the remaining time of time step k .

The state machine in Fig. 5 indicates nine processing states and one *Default* (waiting) state. Here, a fourth order system is used to incorporate two modeled eigenmodes. The matrices with their coefficient nomenclature are consistent with Equation 3. The modal form allows balanced internal numerical values of each state/eigenmode:

$$\mathbf{A} = \begin{bmatrix} \mathbf{A}_1 & \mathbf{0} \\ \mathbf{0} & \mathbf{A}_2 \end{bmatrix}, \text{ where } \mathbf{A}_i = \begin{bmatrix} a_{i,11} & a_{i,12} \\ a_{i,21} & a_{i,22} \end{bmatrix}, \quad (11)$$

$$\mathbf{B} = \begin{bmatrix} b_1 \\ b_2 \\ b_3 \\ b_4 \end{bmatrix}, \mathbf{C} = \begin{bmatrix} c_1 \\ c_2 \\ c_3 \\ c_4 \end{bmatrix}^T, \mathbf{K} = \begin{bmatrix} k_1 \\ k_2 \\ k_3 \\ k_4 \end{bmatrix}^T. \quad (12)$$

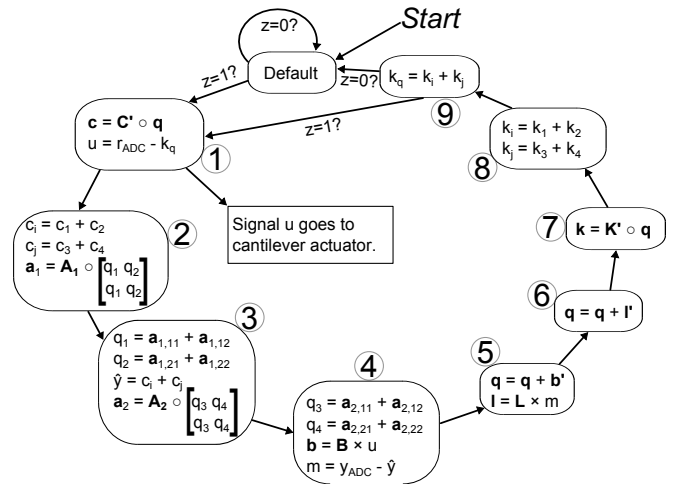


Fig. 5: State machine implementation of the multi-eigenmode compensator for a 4th order system.

Upon start, the state machine enters at the *Default* state. If a new sample is available ($z = 1$), the state machine proceeds from the *Default* state to state 1, or directly from state 9 to state 1. Otherwise, it executes the *Default* state as often as it is awaiting a new sample. r_{ADC} and y_{ADC} are the actuation (reference) r_k and cantilever sensor y_k signal, respectively. Certain new variables are introduced to store intermediate values, as some calculations require more than one operational step. Then, they are distributed on two or more states. Here, c_i , k_q , k_i , $a_{i,xx}$, etc. are such variables. Bold variables indicate vectors or matrices. For example, the operation $\mathbf{b} = \mathbf{B} \cdot u$ are four multiplications carried out by four multipliers in parallel and stored in four intermediate variables indicated as \mathbf{b} . The transpose is indicated by

an apostrophe. The symbol \circ indicates the Hadamard product, an element-wise operation that multiplies the corresponding elements according to $(A \circ B)_{ij} = A_{ij} \cdot B_{ij}$. In the Virtex 5 the *Slow Loop* has a clock rate of 52 MHz, resulting in a compensator feedback loop rate of 5.8 MHz.

Fig. 6 shows various experimental frequency sweeps of the first two transverse eigenmodes with the modified Q_i 's as indicated. The actuation voltage results in different vibration amplitudes in each eigenmode. The interferometric determined values are indicated by gray ordinates, with arrows pointing towards the respective eigenmode. This cantilever with its modified dynamics is used in the following experimental section.

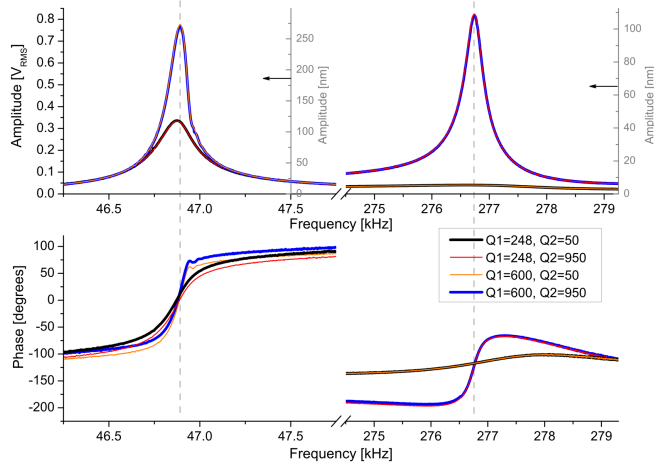


Fig. 6: Experimental modification of Q_1 and Q_2 in the indicated combinations and colors. The tip amplitude in nanometers is also shown.

V. EXPERIMENTAL RESULTS

The imaging and material characterization performance of the bimodal and higher harmonic methods in combination with the multi-eigenmode compensator are investigated. For this, the modified AFM setup of Fig. 1 and cantilever presented in Fig. 6 are used. The first sample utilized is a Bruker PS-LDPE-12M, a two component polymer blend. The Polystyrene (PS) and Polyolefin Elastomer (LDPE) regions have Young's moduli of about 2 GPa and 0.1 GPa, respectively.

The polymer sample is imaged with different combinations of Q_1 and Q_2 (Fig. 7). The type of responses captured are indicated. All images are within the same scan area of the sample, which is $(10 \mu\text{m})^2$ at a scan rate of 2 lines/s. The cantilever amplitude set-points are 50%. Fig. 7 (a) and (b) are the topography and phase (ϕ_1) obtained with the first eigenmode and the natural $Q_1 = 248$ at an actuation frequency of 46.848 kHz. At $Q_1 = 42$ (not shown) the topography appears squeezed due to the higher tip-sample forces. However, the phase has not indicated a higher contrast.

Images with responses of the second eigenmode/6th harmonic and natural $Q_1 = 248$ and $Q_2 = 318$ are

presented in Fig. 7 (c)-(e). Note that the excited 6th harmonic is $6 \cdot \omega_{r,1}$ and usually close to $\omega_{r,2}$.

In Fig. 7 (f)-(h) the Q factors are set to $Q_1 = 42$ and $Q_2 = 950$. This particular combination enables pronounced responses and contrast of the higher eigenmode and harmonic. In contrast to Fig. 7 (c)-(e), respectively, these images indicate a strong improvement in material contrast. In particular ϕ_2 of the bimodal method and the 6th harmonic have pronounced sub-features on the soft LDPE half-spheres. These are less pronounced in the A_2 amplitude image (Fig. 7(f)). Also, they are not visible in the topography and ϕ_1 images of the first eigenmode (Fig. 7 (a) and (b)). In bimodal imaging, this strong effect on A_2 and ϕ_2 can be accounted to the increased second eigenmode's sensitivity to dissipative forces of the sample's materials. Hence, the images form a dissipation map of the different polymers. In the image of the 6th harmonic, dark areas indicate an increased contact time. It results in smaller excited harmonics, as it is the case for the softer LDPE.

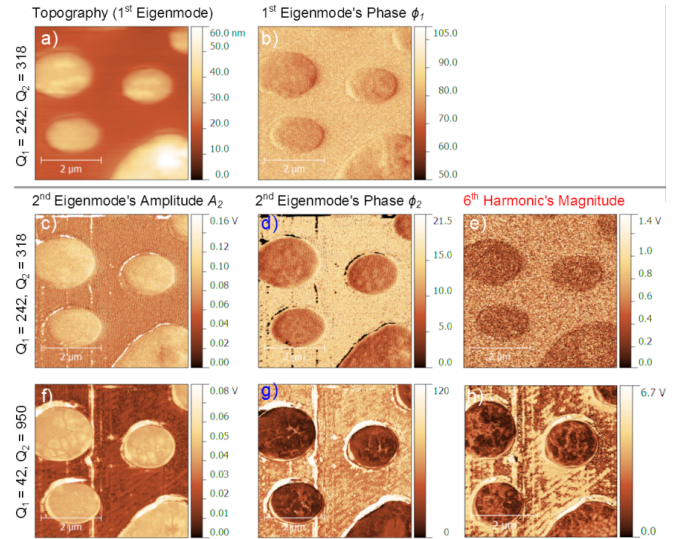


Fig. 7: (a) and (b) are the topography and ϕ_1 (degrees) by using the natural Q_1 and Q_2 . (c),(d) and (e) are images of A_2 and ϕ_2 of the second actuated eigenmode, and the 6th harmonic's signal, respectively, with natural Q_1 and Q_2 . (f),(g) and (h) are obtained in a similar way as (c),(d) and (e), respectively, but with $Q_1 = 42$ and $Q_2 = 950$.

Beside the enhanced material contrast, the combination of a low Q_1 and high Q_2 has an additional advantage. As the first eigenmode is used for the topography feedback mapping, a low Q_1 has an increased imaging bandwidth. This results in faster tracking speed and thus image acquisition, but with increased tip-sample forces. Such high interaction forces can potentially damage the tip and sample. Hence, a trade-off between gentle and fast imaging is required. Fig. 8 is a scan of a calibration sample (Anfatec UMG03/PtS) that has $2 \mu\text{m}$ wide and

58 nm high parallel SiO_2 lines on a silicon substrate with a pitch of $4\ \mu\text{m}$. The scan rate is 15 line/s and the different Q_1 's are indicated. The tracking issues at the higher $Q_1 = 120$ are visible and the lower Q_1 's are clearly superior in following the steps. At $Q_1 = 10$ the increased tip-sample force results in a reduced step resolution.

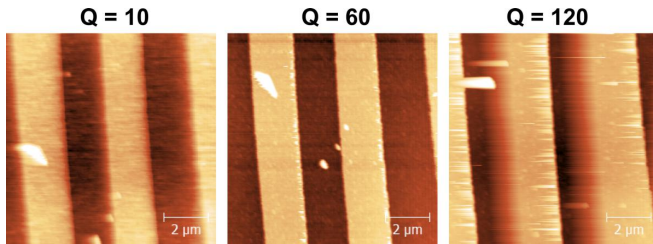


Fig. 8: Sample imaged at 15 lines/s with different Q_1 's.

VI. CONCLUSION

We have demonstrated enhanced material sensitivity achieved by the modification of each cantilever eigenmode's dynamics. In the past, most approaches have addressed a single eigenmode only, typically the first one. However, past research has also shown that higher eigenmodes are more sensitive to the surface force gradients. Here, the appealing combination of Q control with bimodal and higher harmonic methods offers a flexible imaging scheme. The presented approach is able to modify the cantilever dynamics in each eigenmode individually. The resulting digital compensator is used to demonstrate its effectiveness towards enhanced material contrast. Features become visible that were not detected without the compensator. The most pronounced contrast is achieved with a low $Q_1 = 42$ and high $Q_2 = 950$. In addition, a low Q_1 offers high speed imaging capabilities. Hence, the presented approach concurrently improves imaging rates and material contrast obtained with the higher eigenmodes/harmonics. The compensator offers a high flexibility for setting desired imaging conditions and eases the requirement to find a trade-off between sensitivity and imaging speed.

REFERENCES

- [1] Osamah M., El Rifai and K. Youcef-toumi, "Trade-offs and performance limitations in mechatronic systems: a case study," *Annual Reviews in Control*, vol. 28, no. 2, pp. 181–192, 2004.
- [2] A. J. Fleming, B. J. Kenton, and K. K. Leang, "Bridging the gap between conventional and video-speed scanning probe microscopes," *Ultramicroscopy*, vol. 110, no. 9, pp. 1205–1214, 2010.
- [3] T. Sulchek, R. Hsieh, J. D. Adams, G. G. Yaralioglu, S. C. Minne, C. F. Quate, J. P. Cleveland, A. Atalar, and D. M. Adderton, "High-speed tapping mode imaging with active Q control for atomic force microscopy," *Applied Physics Letters*, vol. 76, p. 1473, 2000.
- [4] M. B. Viani, T. E. Schaeffer, A. Chand, M. Rief, H. E. Gaub, and P. K. Hansma, "Small cantilevers for force spectroscopy of single molecules," *Journal of Applied Physics*, vol. 86, no. 4, p. 2258, 1999.

- [5] T. Michels, E. Guliyev, M. Klukowski, and I. W. Rangelow, "Micromachined self-actuated piezoresistive cantilever for high speed SPM," *Microelectronic Engineering*, vol. 97, pp. 265–268, 2012.
- [6] D. Ebeling, H. Holscher, H. Fuchs, B. Anczykowski, and U. D. Schwarz, "Imaging of biomaterials in liquids: a comparison between conventional and Q-controlled amplitude modulation ('tapping mode') atomic force microscopy," *Nanotechnology*, vol. 17, no. 7, pp. S221–6, 2006.
- [7] B. Orun, S. Necipoglu, C. Basdogan, and L. Guvenc, "State feedback control for adjusting the dynamic behavior of a piezoactuated bimorph atomic force microscopy probe," *Review of Scientific Instruments*, vol. 80, p. 063701, 2009.
- [8] J. P. Cleveland, B. Anczykowski, a. E. Schmid, and V. B. Elings, "Energy dissipation in tapping-mode atomic force microscopy," *Applied Physics Letters*, vol. 72, no. 20, p. 2613, 1998.
- [9] R. Garcia, C. Gomez, N. Martinez, S. Patil, C. Dietz, and R. Magerle, "Identification of Nanoscale Dissipation Processes by Dynamic Atomic Force Microscopy," *Physical Review Letters*, vol. 97, no. 1, pp. 1–4, 2006.
- [10] R. W. Stark, T. Drobek, and W. M. Heckl, "Tapping-mode atomic force microscopy and phase-imaging in higher eigenmodes," *Applied Physics Letters*, vol. 74, no. 22, p. 3296, 1999.
- [11] A. Ulcinas and V. Snitka, "Intermittent contact AFM using the higher modes of weak cantilever," *Ultramicroscopy*, vol. 86, no. 1-2, pp. 217–22, 2001.
- [12] R. Garcia and E. T. Herruzo, "The emergence of multifrequency force microscopy," *Nat Nano*, vol. 7, no. 4, pp. 217–226, 2012.
- [13] R. Proksch, "Multifrequency, repulsive-mode amplitude-modulated atomic force microscopy," *Applied Physics Letters*, vol. 89, no. 11, p. 113121, 2006.
- [14] S. D. Solares and G. Chawla, "Frequency response of higher cantilever eigenmodes in bimodal and trimodal tapping mode atomic force microscopy," *Measurement Science and Technology*, vol. 21, no. 12, p. 125502, 2010.
- [15] R. Guckenberger, "Spectroscopy of the anharmonic cantilever oscillations in tapping-mode atomic-force microscopy," *Applied Physics Letters*, vol. 77, no. 20, pp. 3293–3295, 2000.
- [16] A. Raman, S. Trigueros, A. Cartagena, Stevenson, A. P. Z., M. Susilo, E. Nauman, and S. A. Contera, "Mapping nanomechanical properties of live cells using multi-harmonic atomic force microscopy," *Nature Nanotechnology*, vol. 6, no. 12, pp. 809–814, 2011.
- [17] O. Sahin, C. F. Quate, O. Solgaard, and F. J. Giessibl, "Higher Harmonics and Time-Varying Forces in Dynamic Force Microscopy," in *Springer Handbook of Nanotechnology*, B. Bhushan, Ed. Springer Berlin Heidelberg, 2010, pp. 711–729.
- [18] R. W. Stark, "Spectroscopy of higher harmonics in dynamic atomic force microscopy," *Nanotechnology*, vol. 15, no. 3, pp. 347–351, 2004.
- [19] K. S. Karvinen and Moheimani, S O R, "Control of the higher eigenmodes of a microcantilever: applications in atomic force microscopy," *Ultramicroscopy*, vol. 137, pp. 66–71, 2014.
- [20] M. G. Ruppert, M. W. Fairbairn, and S. O. R. Moheimani, "Multi-mode resonant control of a microcantilever for Atomic Force Microscopy," in *2013 IEEE/ASME International Conference on Advanced Intelligent Mechatronics (AIM)*, pp. 77–82.
- [21] R. Pedrak, T. Ivanov, K. Ivanova, T. Gotszalk, N. Abedinov, I. W. Rangelow, K. Edinger, E. Tomerov, T. Schenkel, and P. Hudek, "Micromachined atomic force microscopy sensor with integrated piezoresistive sensor and thermal bimorph actuator for high-speed tapping-mode atomic force microscopy phase-imaging in higher eigenmodes," *Journal of Vacuum Science & Technology B: Microelectronics and Nanometer Structures*, vol. 21, no. 6, p. 3102, 2003.
- [22] T. Ivanov, T. Gotszalk, T. Sulzbach, and I. W. Rangelow, "Quantum size aspects of the piezoresistive effect in ultra thin piezoresistors," *Ultramicroscopy*, vol. 97, no. 1-4, pp. 377–384, 2003.
- [23] L. Ljung, *System identification: Theory for the user*, 2nd ed. Upper Saddle River, NJ: Prentice Hall, 1999.